Revista de La Facultad de Ciencias de la UNI, REVCIUNI 15 (1) (2012) 7-15

Direct profiling of polarization fields in nitride semiconductors at nanometric scale using electron holography in the transmission electron microscope

F A Ponce
Department of Physics, Arizona State University, Tempe, AZ 85287-1504, USA

E-mail: ponce@asu.edu

Abstract:The nitride semiconductors are widely used in high efficiency light emitting devices and are currently being considered for photovoltaic applications. The reduced symmetry in the wurtzite structure compared to cubic semiconductors results in the growth of large densities of crystalline defects and in the presence of strong spontaneous and piezoelectric polarization effects. A correlation between the microstructure and the polarization fields can be achieved with electron holography in the transmission electron microscope. Electron holograms thus obtained can provide energy band profiles with sub-nanometer spatial resolution. The phase of the electron beam is sensitive to the electrostatic potential, and a direct measurement of the latter can be achieved by making the electron beam signal that traverses the specimen interfere with a reference electron beam that travels through vacuum. This technique has been quite useful in probing the fields and charges at dislocations and at interfaces in semiconductors, and it is particularly useful to determine the piezoelectric effects in group III nitride semiconductor heterostructures. A review of applications to InGaN and AlGaN based heterostructures is presented in this paper.

Key words:Electron energy band profiles, piezoelectric fields, nitride semiconductors, electron holography

1. Introduction

In the past two decades, the nitride semiconductors have acquired pronounced relevance due to their robustness and their range of band gaps[1]. The bond between nitrogen and the group III elements is strong; the cohesive energies of AlN, GaN, and InN are 11.67, 9.06, and 7.97 eV, respectively.[2] The corresponding band gap energies of 6.28, 3.41, and 0.7eV span the electromagnetic spectrum from the infrared into the ultraviolet, including the full visible spectrum.[3] The growth of these materials is challenging due to the high temperatures required for synthesis and the absence of suitable substrates. High densities of dislocations are necessary in order to accommodate the lattice mismatch and the thermal expansion mismatch within the AlGaInN alloy system.[4] The lattice displacement is associated with those dislocations (Burgers vectors) are large compared with the interatomic bond length.[5]Heterojunction lattice mismatch often results in pseudomorphic thin film structures with large strain fields.[6-9] The absence of a center of symmetry in the hexagonal wurtzite structure results in significant spontaneous polarization. In addition, piezoelectric polarization results from the strain due to dislocations and strained heterointerfaces. The electrostatic fields due to spontaneous and piezoelectric polarization are of the order of several MeV/cm,[7] and are typically highly localized at the nanometer scale, and have a strong effect on carrier transport and carrier recombination.

Profiles with nanometer resolution of the electrostatic potential and charge distribution in solids can be obtained by electron holography in the TEM. This technique has been used to visualize the potential energy profile across p-n junctions in silicon devices used in microelectronics.[10] Electron holography has been particularly useful to measure the potential and charge density variations in the

nitride semiconductors. Electron holography was first used by Cherns in 1999 to measure the piezoelectric field in InGaN quantum wells.[11] In this paper, a brief introduction is first given to the electron holography technique. This is followed by examples of applications to determine the nature of electrostatic potential variations in the vicinity of dislocations in GaN, at InGaN/GaN quantum wells, and at two-dimensional electron and hole gas heterostructures.

2. Electron holography in the transmission electron microscope

The use of electron holography has increased significantly in the last decade, particularly in the direct measurement of the electrostatic fields and charges in nitride semiconductor materials. In conventional TEM techniques, like those used for diffraction contrast analysis, only the intensity of the electron beam is recorded, while the phase information is lost. Electron holography is an interferometric technique which provides information about spatial distribution of the phase shift, $\Delta\theta$. In order to obtain the phase information, a highly coherent electron beam is obtained by using a field emission gun. A sample is prepared to electron transparency, but not too thin to avoid surface related effects such as strain relaxation and screening due to the surface.

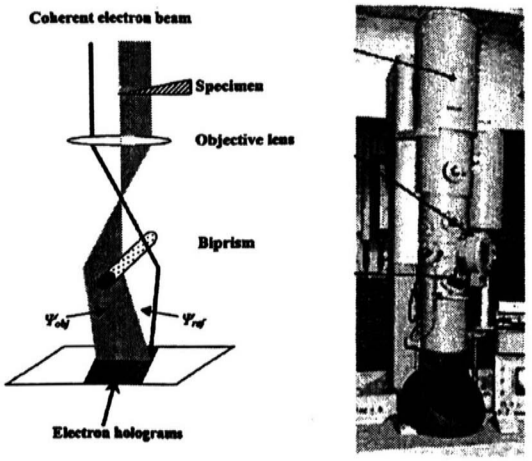

Figure 1. Schematic diagram of the electron beam path for electron holography in a transmission electron microscope.

The phase of the electron beam is modulated by spatial variations of the electrostatic potential of the specimen. Figure 1 shows the configuration used for electron holography. The sample is introduced into the electron beam path covering about half of the beam diameter. The other half of the beam travels through vacuum and it is used as a reference beam. The electrons that traverse the sample experience a change in velocity, in part due to the variation of the reference potential, and gain in phase compared to the electrons traveling through vacuum. The phase change is directly proportional to the electrostatic potential as we will see later. The phase information can be retrieved from the wave interference pattern.[12,13]

Electron holography is an electron-interference technique that makes the recovery of the phase information possible. A conducting filament that acts as an optical biprism is used to produce an interference pattern. The biprism is aligned manually so that its image matches the boundary of the specimen at the image plane. When a positive bias is applied to the biprism, the beams traveling through vacuum (reference wave) and the sample (object wave) are made to overlap at the image plane, and their overlap is recorded. The geometric configuration around the biprism is depicted in Fig. 2(a). The biprism filament is along the y-direction, and the beam propagates along the z-direction. The biprism is at a given potential, while the two plates are grounded. In some microscopes these two plates are the edges of the selected area aperture.

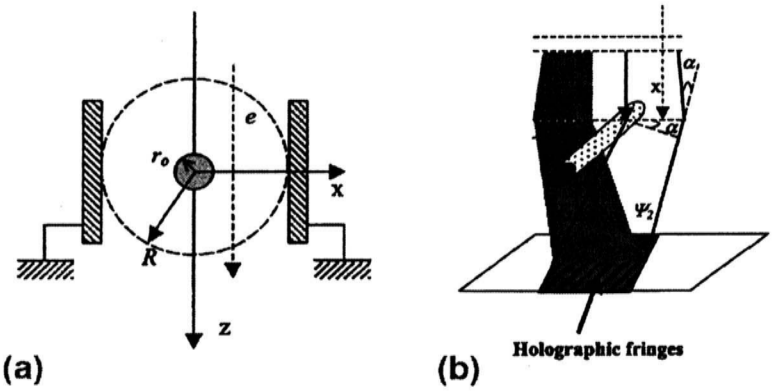

Figure 2. Holographic image formation. (a) configuration around the biprism: (b) Interference between two plane waves.[13]

As already indicated, the specimen under investigation is positioned to cover only half of the object plane, in that way one beam passes through the specimen (referred as the object wave$\psi_{obj} = A_o e^{i\theta_o}$) and the other beam passes through the vacuum (referred to as the vacuum wave$\psi_{vac} = A_v e^{i\theta_v}$). A bi-prism, which resides in the plane of the selected area aperture, deflects the two electron beams in order to cause their interference. Applying a positive bias to the filament of the bi-prism, the object wave and vacuum wave converge and yield an interference pattern in the overlapping region. The intensity distribution can be represented by: [13]

$$I = \left| A_v e^{i(\theta_v - \Delta)} + A_o e^{i(\theta_o + \Delta)} \right|^2$$
$$= A_v^2 + A_o^2 + 2A_v A_o \cos(\theta_o - \theta_v - 2\Delta)$$

where the first two terms represent the background intensity and the third terms represent the superimposed interference fringes. The extra phase shiftΔ is due to the biprism deflection, which is dependent on the applied field and the geometric configuration of thebiprism, but is not a property of specimen. The information that we want to obtain is the phase shift θ_o - θ_v which is due to the modulation by the crystal potential V. The crystal electrostatic potential V is typically in the order of 10eV which is much less than the electron beam energy, so that the difference of momentum between object and vacuum waves is proportional to V. Considering relativistic effects, the relationship between phase shiftθ_o - θ_v and crystal potential V is:

$$\theta_o - \theta_v = \int \frac{p_{obj} - p_{vac}}{\hbar} dz = \frac{eV(E - E_0)}{E(E + 2E_0)} \frac{2\pi t}{\lambda}$$

where$E$ is the kinetic energy of incident electron beam, E_o is the rest energy of electron, t is specimen thickness and λ is the wavelength of electron beam. With a fixed accelerating voltage in the TEM, this expression can also be written as:

$$\theta_o - \theta_v = C_E V t,$$

whereC_E is a constant. Therefore, the crystal electrostatic potential profile can be obtained from the phase shift information that is extracted from the electron hologram.

The phase reconstruction process[12] starts by taking the Fourier transform of the intensity equation shown above. Three delta functions appear, involving convolutions represented by the symbol $\otimes$

$$FT(I) = \delta(q) \otimes FT(A_v^2 + A_v^2) + \delta(q - q_\Delta) \otimes FT\left(A_v A_o e^{i(\theta_v - \theta_o)}\right) + \delta(q + q_\Delta) \otimes FT\left(A_v A_o e^{-i(\theta_v - \theta_o)}\right)$$

The background intensity is transferred into an autocorrelation function and appears to be in the center, while the Fourier transform of the co-sinusoidal interference fringes provides two sidebands, which are away from center by the carrier spatial frequency, q_Δ. The next step is to shift one of the sidebands to the center, and take the inverse Fourier transform. A complex object image with a modulusA_vA_o and phase θ_o - $\theta_v$is obtained. In addition, if we remove the specimen and take the hologram, a complex image with a modulus A_v^2 and zero phase shift can be obtained. The damping of amplitude of the electron beam across the specimen is due to the inelastic scattering process in the material and can be expressed as

$$\frac{A_o}{A_v} = e^{-t/2\lambda_i}$$

where$\lambda_i$hereis the mean free path for inelastic scattering of electrons in the crystal. Therefore, the thickness profile of a specimen can be obtained from the amplitude image, while the electrostatic potential profile of the specimen can be obtained from the phase image. Furthermore, in a one-dimensional potential profile, the internal fields are proportional to the slope of the electrostatic potential. The corresponding electrostatic charges are found using Poisson's equation, and are related to the curvature of the potential profile.

3. Dislocations in GaN

As mentioned before, thin epitaxial films with optimized electronic properties have threading dislocation densities ranging from 10^8 to 10^{10} cm^{-2}.[4] They play an important role in accommodating epitaxial growth under adverse conditions associated with lattice mismatch and thermal mismatch with the substrate and at InAlGaN compound heterojunctions. Threading dislocations have been found to be of the edge, screw, and mixed types.[14] The Burgers vectors of the dislocations are large with respect to the lattice parameters, which often leads to the formation of coreless dislocations.[15] Dislocations are frequently associated to non-radiative recombination centers.[16] The electrostatic charges at dislocations lines were first studied using electron holography by Cherns[17] and Cai.[18]They found that dislocations have specific charges depending on the dislocation type.

4. Polarization fields in InGaN/GaN

In the absence of a center of symmetry, the hexagonal wurtzite structure exhibits noticeable spontaneous and piezoelectric polarization effects.[7] Polarization fields up to a few MeV/cm in the nitride semiconductors were first determined by applying a reverse bias to the p-n junction,[8] and later by electron holography.[11] The strong internal field can lead to positive and detrimental effects in light emitting diodes (LEDs). Reduced radiative recombination efficiency can result from the spatial separation of electrons and holes. Spatially separated by the Stark effect, their transition matrix elements and the radiative recombination rate can be significantly decreased. In addition, the internal fields facilitate the escape of carriers and reduce the carrier capture cross section by quantum wells.

Another detrimental effect is instability of the emission wavelength for devices operating under high injection conditions. The polarization field is screened and the emission wavelength is blue-shifted. The magnitude of this shift could be up to 100nm for large polarization cases, such as for InGaN/GaN green LEDs. Therefore, it is important to find ways to prevent polarization effects in the active region. Non-polar and semi-polar growth have been proposed and their fabrication has been successfully demonstrated. However, the in-plane polarization could still be a problem for the non-polar growth of quantum wells, as we will see later.

On the other hand, strong polarization fields could play a positive role in the conductivity of p-region and n-region in LEDs. In n-type AlGaN/GaNheterostructures, the positive polarization sheet charges at the interface will promote the formation of two-dimensional electron gas (2-DEG) with a sheet carrier concentration as high as 10^{13} cm^{-2}. Similarly in p-type AlGaN/GaNheterostructures, the negative polarization sheet charges at the interface could help with the formation of two-dimensional hole gas (2-DHG). By substituting the conventional n-GaN or p-GaN layer in LEDswith the proper AlGaN/GaN multi-heterostructure, the lateral conductivity of LEDs can be enhanced, and an

improved current spreading can be expected.

In the following sections, we discuss the theoretical aspect of the polarization field in nitrides, and then the measurement of polarization effects by electron holography, including the mapping of internal electrostatic potential in the InGaN/GaN quantum wells and evidence of the formation of 2-DEG and 2-DHG in n-type and p-type AlGaN/GaNheterostructures, respectively.

5. Electrostatic fields and charges in light emitting diodes emitting in the green region of the visible spectrum

Various aspects of polarization fields in InGaN/GaN quantum wells have been reported[6-9]and measured.[19-21]In particular, there is much interest in the polarization field and charge distribution in InGaN/GaN multi-quantum wells in the active region of green LEDs. An important feature of electron holography is that it can provide a mapping of the electrostatic potential distribution at an atomic scale, while other techniques usually give average values. An example of a green LED structure is shown in Fig. 3.[22] This layer structure was grown by metal organic chemical vapor deposition on a c-plane sapphire substrate, the active region containing five InGaN/GaN quantum well periods, emitting light at ~2.3 eV. Cross- section samples were prepared for TEM using standard mechanical polishing and argon-ion milling techniques. Figure 3(a) is a high-resolution image of the active region. The InGaN QW and GaN barriers are uniform with a thickness of 4.6 and 9.3 nm, respectively. The interfaces are flat and atomically abrupt.

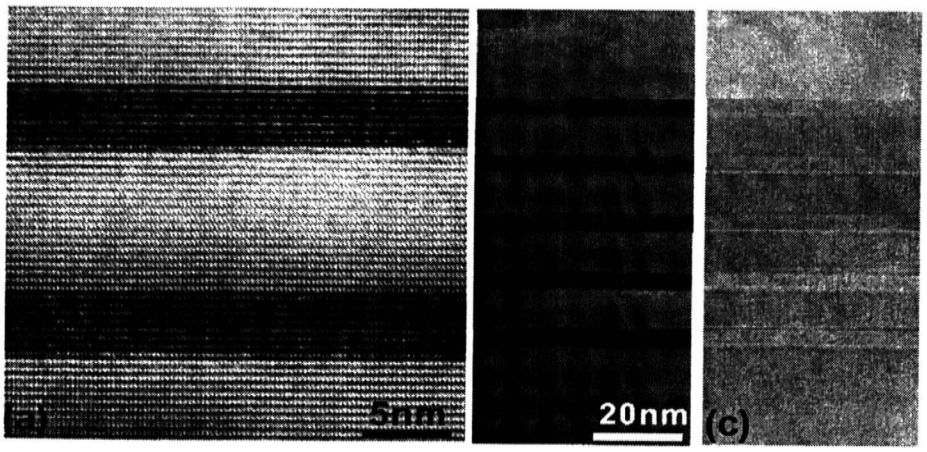

Figure 3. Active region of a green LED. (a) High resolution TEM of the quantum well region. (b) Electrostatic potential profile showing the p-n junction and quantum well region. (c) Charge density distribution due to polarization effects.[22]

Electron holograms of the active region were obtained with the sample aligned to minimize diffraction conditions while keeping close to an orientation where the electron beam was parallel to the interfaces. The holograms were digitally recorded using a charge coupled device camera. The amplitude and phase values were deconvoluted from the electron hologram; the results are shown in Figs. 3(b) and 3(c). The resulting spatial profile of the electrostatic potential and charge distribution are plotted in Fig. 4. The electrostatic potential distribution due to the p-n junction is clearly observed in Fig. 4(a) with a shift of about 3 eV in the conduction band edge. Also observed is the potential profile due to the quantum wells. It is noticed that the field and the polarization charge density in the quantum wells vary with distance to the p-n junction. The sheet polarization charge densities of the first three InGaN quantum wells have a similar value of ~ 0.018 C/m^2, corresponding to a 20% indium composition, for a non-screening case, and corresponding to piezoelectric fields of ~1.95 MV/cm. The sheet polarization charge densities in the fourth and fifth periods are estimated to be 0.007 and 0.0005 C/m^2, respectively. This corresponds to a significant screening of the fourth and fifth QWs.

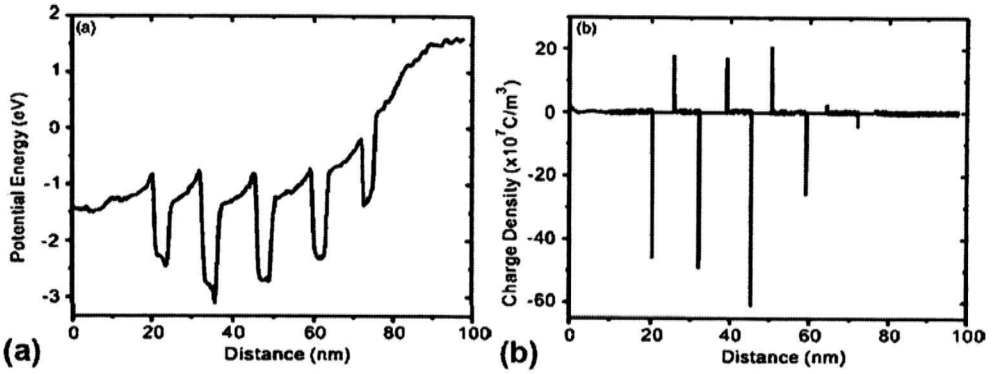

Figure 4. Active region of a green LED. (a) Electrostatic potential profile showing the p-n junction and quantum well region. (b) Charge density distribution due to polarization effects.[22]

The observation of inhomogeneous polarization fields within the multi-quantum well is consistent with a depth-resolved study using cathodoluminescence,[22] in which a low energy peak appears when the accelerating voltage is increased. The decay of piezoelectric fields in the fourth and fifth QWs could be due to strain relaxation. It is possible that the first three periods remain fully strained while the fourth and fifth periods undergo plastic relaxation. Another possibility involves the migration of hydrogen ions from the p-type region into the top two QWs.

6. Two-dimensional electron gas (2DEG) thin film structures

Strong polarization fields can result in two-dimensional carrier confinement, also known as two-dimensional electron gas (2DEG), in AlGaN/AlN/GaNheterostructures. The high electron conductivity of these thin film structures can be used to provide low resistant current paths to n- and p-type layers of the LED.[23-26] Fig. 5 shows part of a n-type AlGaN/AlN/GaNsuperlattice, exhibiting 2-D electron gas at the AlN/GaN interface. The AlGaN/AlN/GaNsuperlattice was epitaxially grown by MOCVD on an n-doped 10^{18} cm^{-3}, 3μmGaN layer on a c-plane sapphire substrate. The SL consists of 11 periods; each period starts with a 0.5 nm AlN layer, followed by a 12 nm AlGaN barrier layer with an Al concentration that is nominally graded linearly from 30% to 0%, and ends with a 28 nm GaN layer. The AlN layer is used to avoid interface alloy scattering effects and to improve the lateral mobility of the 2-DEG. Using a very thin AlN layer prevents significant reduction of the vertical conductivity. The AlGaN layer has an n-type doping level of 2×10^{19} cm^{-3}, and the n-type GaN in the SL is doped at 2×10^{18} cm^{-3}. In order to avoid impurity scattering, doping of the AlGaN layer was delayed by 4 s during growth, i.e., the first nanometer of the AlGaN is undoped; and the doping of the GaN layer was stopped 10 nm before starting the growth of the next AlN/AlGaN barrier. The characteristics of the full superlattice are observed in Fig.5(a). A higher magnification TEM image showing the two top periods of the SL structure is shown in Fig. 5(b). The AlN layer appears with the brightest contrast, followed by the graded AlGaN layer with fading brightness and the GaN layer with relatively darker contrast.

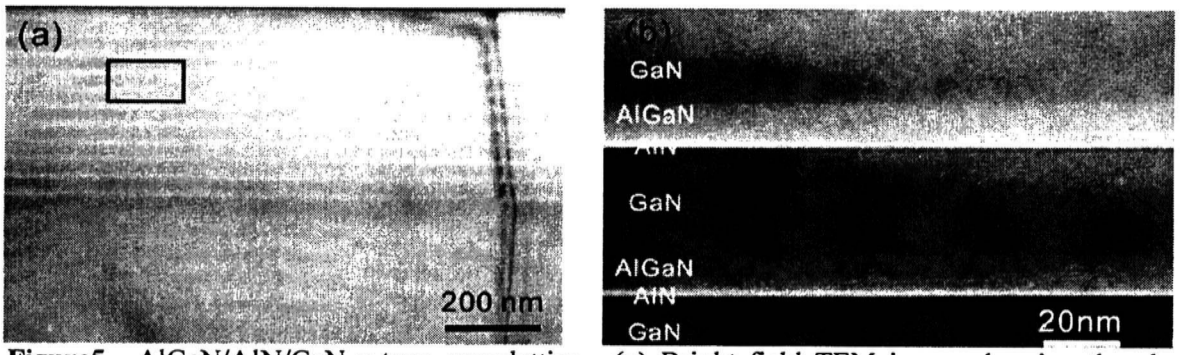

Figure5. AlGaN/AlN/GaN n-type superlattice. (a) Bright field TEM image showing the eleven periods. (b) Higher magnification TEM image showing the top two periods. [24]

The electrostatic potential distribution obtained from the reconstructed phase and amplitude images are shown in Fig.6(a). A profile with higher spatial resolution is shown in Fig. 6(b). An energy dip close to the GaN/AlN interface represents the accumulation of the 2-DEG. The curvature of the potential around the 2-DEG region is negative as expected. These results are consistent with calculated energy band diagrams. [25]

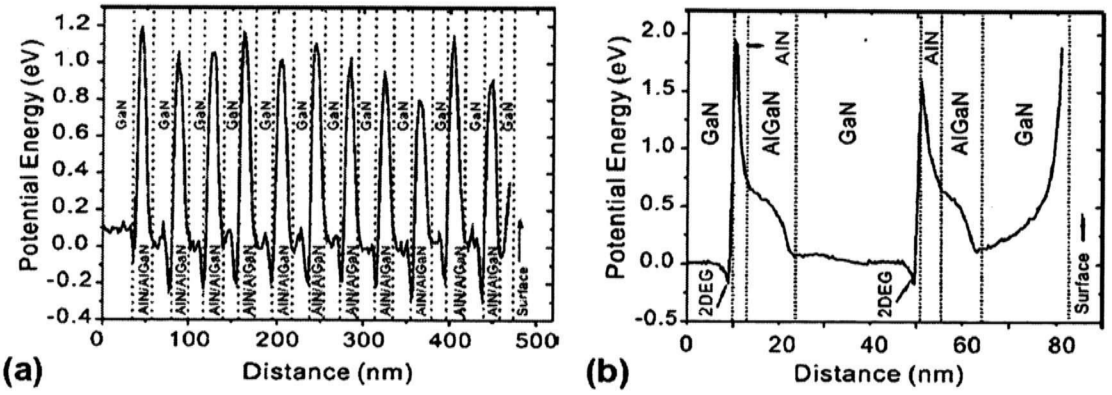

Figure 6. Potential energy profiles of AlGaN/AlN/GaN n-type superlattice showing the features of the 2DEG in the complete superlattice (a) and in the top two periods (b). [24]

7. Two-dimensional electron gas (2DHG) structures

If the AlGaN/GaN multi-heterostructure is made p-type, the band diagram would be different from the n-type case due to the alignment of Fermi-level. In order to achieve the accumulation of a 2-DHG, the growth sequence of GaN/AlN/AlGaN should be adjusted and the device structure should be optimized. We have studied a p-type AlGaN/GaN multi-heterostructure, which is designed for the purpose of high conductivity with the accumulation of 2-DHG. [25-26]

The AlGaN/AlN/GaNheterostructure in Fig. 7 was epitaxially grown by metal-organic chemical vapor deposition on a nominally un-doped 3-μm thick GaN layer on a c-plane sapphire substrate. The 2-DHG heterostructure consists of 6 periods; each period starts with a 0.5 nm AlN layer, followed by a 5 nm nominally un-doped GaN layer, and ending with a 12 nm AlGaN barrier layer with an aluminum concentration that is nominally graded linearly from 0% to 10%. The thin AlN layer is used to avoid interface alloy scattering effects and to improve the lateral mobility of the 2-DHG. In order to optimize the vertical conductivity, a very thin AlN layer is used. The initial portion of the AlGaN layer has a Mg doping level of $\sim 1\times10^{19}$ cm^{-3}, but the Mg flux is turned off for the last few nanometers. The nominally un-doped GaN shows, in secondary ion mass spectroscopy, a Mg background concentration in the range of $1\text{-}5\times10^{18}$ cm^{-3}, due to memory effects.

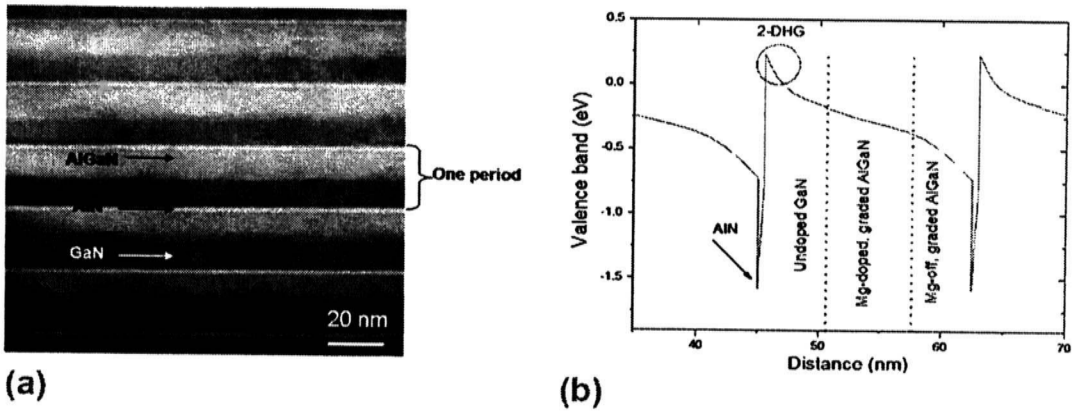

Figure7. AlGaN/AlN/GaNsuperlattice structure. (a) TEM image of the superlattice. Brighter regions indicate high aluminum content. (b) Sketch of valence band profile of one period. The 2-DHG accumulation region is circled. [26]

Fig. 8 shows the electrostatic potential profile for 3 superlattice periods. The locations of the interface are determined by a careful match between diffraction contrast and phase image. The formation of a 2-DHG is revealed by a positive curvature in the GaN immediately to the right of the AlN layer in the potential energy profile. The two-dimensional hole gas (2-DHG) at the interface cancels the spontaneous polarization charges, and no discontinuity in the potential profile is observed. But the depletion of holes produces a positive curvature in the profile, in contrast to a negative curvature in the 2-DEG case.

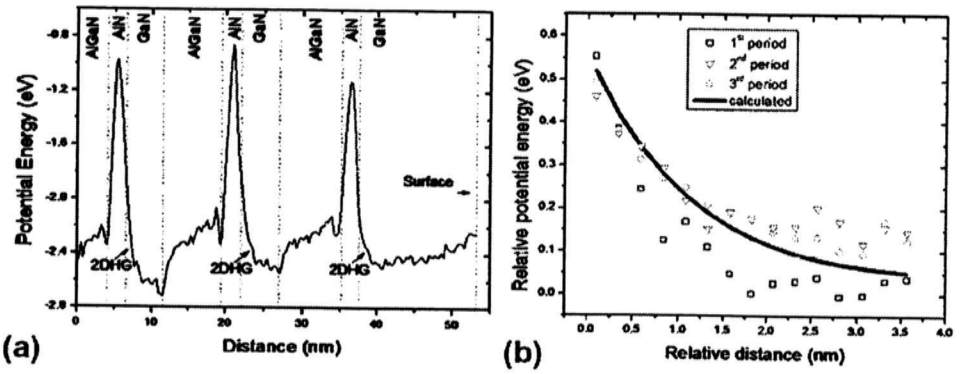

Figure8. Potential profile of an AlGaN/AlN/GaNsuperlattice doped p-type, exhibiting a 2-DHG. No discontinuity is observed at the AlN/GaN interface. [26]

Generally, in semiconductor structures of this type, we find four major types of charges that are responsible for the variations of the electrostatic potential. (1) Fixed charges like those due to spontaneous and piezoelectric polarization, (2) ionized impurities, (3) interface fixed charges (band offset), and (4) free carriers (in our case holes) that redistribute under the effect of the other charges. For the 2-DHG case, the major contribution to the potential variation is from the holes confined on a nanoscale of length. In our case, the experimental and calculated potential distributions both show a noticeable curvature in the vicinity (~1nm) of the interface, but become relatively flat away from the interface, which indicate the 2DHG accumulation happens over only a few atomic monolayers of the interface. [26]

8. Conclusion

Defects and interfaces in the nitride semiconductors are closely related to the electronic and optical properties via the induced polarization fields. A detailed understanding of the electrostatic potential properties of semiconductor structures is possible at near the atomic scale using electron holography in the TEM. A brief introduction to the technique has been presented in this paper, and some applications to the study of electrostatic fields associated with dislocations, quantum wells, and 2DEG and 2DHG heterostructures of nitride semiconductors have beendiscussed. This type of studies is essential in order to achieve high efficiency light emitting devices. Similar studies should also be useful for the development of photovoltaic devices based on these materials.

References

[1] Ponce FA and Bour D P 1997*Nature***386**, 351-9.
[2] Stampfl C and Van de Walle C G 1999 *Phys. Rev. B***59**, 5521-35.
[3] Wu J,Walukiewicz W, Yu K M, Ager III J W, Haller E E, Lu H, Schaff W J, Saito Y, and Nanishi Y 2001*Appl. Phys. Lett.***80** 3967-9.
[4] Lester S D, Ponce FA, Craford M G, and Steigerwald D A 1995 *Appl. Phys. Lett.*66, 1249-51.
[5] Ponce FA, Cherns D, Young W T, and Steeds J W 1996 *Appl. Phys. Lett.***69**, 770-2.
[6] Look D C and Sizelove J R 1999*Phys. Rev. Lett.***82**, 1237-40.
[7] Bernardini F, Fiorentini V, and Vanderbilt D 1997*Phys. Rev. B***56**, R10024-28.
[8] Takeuchi T, Wetzel C, Yamaguchi S, Sakai H, Amano H, Akasaki I, Kaneko Y, Nakagawa S, Yamaoka Y, and Yamada H 1998*Appl. Phys. Lett.***73**, 1691-3.
[9] Wei Q Y, Li T, Wu Z H, and Ponce FA 2010*Phys. Stat. Sol. A***207**, 2226-32.
[10] McCartney M R, Smith D J, Hull R, Bean J C, Voelkl E, and Frost B 1994*Appl. Phys. Lett.***65**, 2603-5.
[11] Cherns D, Barnard J, and Ponce FA 1999*Solid State Comm.***111**, 281-5.
[12] McCartney M R and M. Gaidardziska-Josifovska M 1994*Ultramicroscopy***53**, 283-8.
[13] Cai J and Ponce FA 2002*J. Appl. Phys.***91**, 9856-62.
[14] Ponce FA, Cherns D, Young W T, and Steeds J W 1996*Appl. Phys. Lett.***69**, 770-2.
[15] Cherns D, Young W T, Steeds J W, Ponce FA, and Nakamura S 1998*Phil. Mag. A***77**, 273-86.
[16] Ponce FA, Bour D P, Goetz W, and Wright P J 1996*Appl. Phys. Lett.***68**, 57-9.
[17] Cherns D and Jiao C G 2001*Phys. Rev. Lett.***87**, 205504-7.
[18] Cai J and Ponce F A 2002*Phys. Stat. Sol. A***192**, 407-11.
[19] McCartney M R, Ponce FA, Cai J, Bour D P 2000*Appl. Phys. Lett.***76**, 3055-7.
[20] Cai J, Ponce FA, Tanaka S, Omiya H, and Nakagawa Y 2001*Phys. Stat. Sol. A***188**, 833-7.
[21] Stevens M, Bell A, McCartney M R, Ponce FA, Marui H, and Tanaka S 2004*Appl. Phys. Lett.***85**, 4651-3.
[22] Wu Z H, Fischer A M, Ponce FA, Lee W, Ryou J H, Yoo D, and Dupuis R D 2007 *Appl. Phys. Lett.***91**, 041915.
[23] Wu Z H, Stevens M, Ponce FA, Lee W, Ryou J H, Yoo D, and Dupuis R D 2007 *Appl. Phys. Lett.***90**, 032101.
[24] Wu Z H, Ponce FA, Hertkorn J, and Scholz F 2007*Appl. Phys. Lett.***91**, 142121.
[25] Hertkorn J, Thapa S B, Wunderer T, Scholz F, Wu Z H, Wei Q Y, Ponce FA, Moram M A,Humphreys C J, Vierheilig C, and Schwarz UT 2009 *J. Appl. Phys.***106**, 013720.
[26] Wei Q Y, Wu Z H, Sun K W, Ponce FA, Hertkorn J, and Scholz F 2009*Appl. Phys. Exp.***2**, 121001.